Current Research in Structural Biology 4 (2022) 308–319

Contents lists available at ScienceDirect

Current Research in Structural Biology

journal homepage: www.journals.elsevier.com/current-research-in-structural-biology

Research Article

# Regulation of the interactions between human eIF5 and eIF1A by the CK2 kinase

Nathan Gamble, Eleanor Elise Paul, Bibin Anand, Assen Marintchev *

*Department of Physiology & Biophysics, Boston University School of Medicine, 700 Albany St. W336, Boston, MA, 02118, USA*

ARTICLE INFO

Handling editor: Prof N Ban

*Keywords:*
Translation initiation
eIF5
eIF1A
NMR
Protein-protein interactions
Dynamic interactions

ABSTRACT

Translation initiation in eukaryotes relies on a complex network of interactions that are continuously reorganized throughout the process. As more information becomes available about the structure of the ribosomal preinitiation complex (PIC) at various points in translation initiation, new questions arise about which interactions occur when, their roles, and regulation. The eukaryotic translation factor (eIF) 5 is the GTPase-activating protein (GAP) for the GTPase eIF2, which brings the initiator Met-tRNA$_i$ to the PIC. eIF5 also plays a central role in PIC assembly and remodeling through interactions with other proteins, including eIFs 1, 1A, and 3c. Phosphorylation by casein kinase 2 (CK2) significantly increases the eIF5 affinity for eIF2. The interaction between eIF5 and eIF1A was reported to be mediated by the eIF5 C-terminal domain (CTD) and the eIF1A N-terminal tail. Here, we report a new contact interface, between eIF5-CTD and the oligonucleotide/oligosaccharide-binding fold (OB) domain of eIF1A, which contributes to the overall affinity between the two proteins. We also show that the interaction is modulated by dynamic intramolecular interactions within both eIF5 and eIF1A. CK2 phosphorylation of eIF5 increases its affinity for eIF1A, offering new insights into the mechanisms by which CK2 stimulates protein synthesis and cell proliferation.

## 1. Introduction

Translation initiation in eukaryotes is a multistep process, requiring several proteins called eukaryotic translation initiation factors (eIFs), which form complexes on and off the ribosome. The translation preinitiation complex (PIC) undergoes multiple rearrangements throughout the process. eIF5 is the GTPase-activating protein (GAP) for eIF2, the GTPase responsible for bringing Met-tRNA$_i$ to the PIC. eIF5 has an N-terminal domain (NTD), which performs the GAP function, and a C-terminal domain (CTD), which is responsible for most of the protein-protein interactions, including with the N-terminal tail of the β subunit of eIF2 (eIF2β-NTT) (reviewed in (Hinnebusch, 2014; Jackson et al., 2010; Marintchev and Wagner, 2004; Sonenberg and Hinnebusch, 2009; Weisser and Ban, 2019)). The interaction between eIF5-CTD and eIF2β-NTT is mediated by two acidic/aromatic (AA) boxes in eIF5-CTD and three poly-lysine segments (K-boxes) in eIF2β-NTT (Asano et al., 1999; Yamamoto et al., 2005). eIF5 and eIF2 are part of a multifactor complex (MFC) that forms off the ribosome, which also includes eIFs 1 and 3, and can bind to the PIC as a pre-formed complex. eIF5 mediates several interactions within the MFC and the PIC: with eIFs 1, 1A, 2, and 3c (Asano et al., 2000; Luna et al., 2012, 2013; Obayashi et al., 2017; Sokabe et al., 2012). eIF5 is phosphorylated by Casein Kinase 2 (CK2), at S389 and S390, located in AA-box 2, which leads to stimulation of protein synthesis and cell proliferation (Homma et al., 2005).

eIF1A acts together with eIF5B, another GTPase, to promote ribosomal subunit joining. eIF1A consists of an oligonucleotide/oligosaccharide-binding fold (OB) domain, surrounded by two intrinsically disordered tails, NTT and CTT. eIF1A-CTT dynamically interacts with the OB domain. Upon eIF1A binding to the 40S ribosomal subunit, eIF1A-CTT is displaced from the OB domain and is relocated to the ribosomal P-site (Battiste et al., 2000; Fekete et al., 2005; Lapointe et al., 2022; Nag et al., 2016; Olsen et al., 2003; Saini et al., 2010; Yu et al., 2009). Upon start codon selection, where the PIC undergoes major rearrangements, including release of eIF1, the eIF1A-CTT is displaced from the P-site and is free to contact eIF5B, which promotes ribosomal subunit joining (Acker et al., 2006, 2009; Fringer et al., 2007; Lapointe et al., 2022; Nag et al., 2016; Yu et al., 2009). eIF1A-NTT contacts eIF5-CTD at a surface including AA-boxes 1 and 2 (Luna et al., 2013). The contact interfaces of eIF5-CTD with eIF1, 1A and 3c show significant overlap with the eIF2β-NTT binding surface; therefore, eIF2β-NTT is

* Corresponding author. 700 Albany St. W336, Boston, MA, 02118, USA.
*E-mail address:* amarint@bu.edu (A. Marintchev).

https://doi.org/10.1016/j.crstbi.2022.09.003
Received 30 June 2022; Received in revised form 26 August 2022; Accepted 12 September 2022

presumed to be at least partially displaced from eIF5 within the PIC (Luna et al., 2012, 2013; Obayashi et al., 2017; Paul et al., 2022). eIF5-CTT likely contacts eIF5B in the 43S PIC and is displaced by eIF1A-CTT at some point after start codon selection (Lin et al., 2018). Upon start codon selection, GTP hydrolysis by eIF2 and phosphate release, the resulting eIF2-GDP has lower affinity for Met-tRNA$_i$ and dissociates from the PIC alongside eIF5 (reviewed in (Hinnebusch, 2014; Jackson et al., 2010; Marintchev and Wagner, 2004; Sonenberg and Hinnebusch, 2009; Weisser and Ban, 2019)).

We recently reported that the phosphomimetic mutant of eIF5-CTD (S389E/S390E), mimicking phosphorylation by CK2, significantly increases the affinity of eIF5-CTD for eIF2β-NTT, offering a possible molecular mechanism for the CK2-induced stimulation of protein synthesis and cell proliferation (Paul et al., 2022). The extensive overlap between the contact surfaces in eIF5-CTD for eIF1A and eIF2β, which include AA-box 2, where the CK2 phosphorylation sites are located, suggested that CK2 phosphorylation could also modulate the affinity of eIF5 binding to eIF1A. While performing NMR titrations between eIF1A and eIF5-CTD (Paul et al., 2022), we consistently observed small, but reproducible chemical shift perturbation (CSP) effects in the folded OB domain of eIF1A, in addition to the effects in eIF1A-NTT.

Here we report that the eIF1A-OB domain and eIF5-CTD do indeed contact each other, and that eIF1A-CTT interferes with this interaction. Quantitative binding assays show that the interaction of eIF5-CTD with the OB domain of eIF1A in the absence of the eIF1A-CTT contributes to the affinity of eIF5 for eIF1A. We go on to show that the phosphomimetic

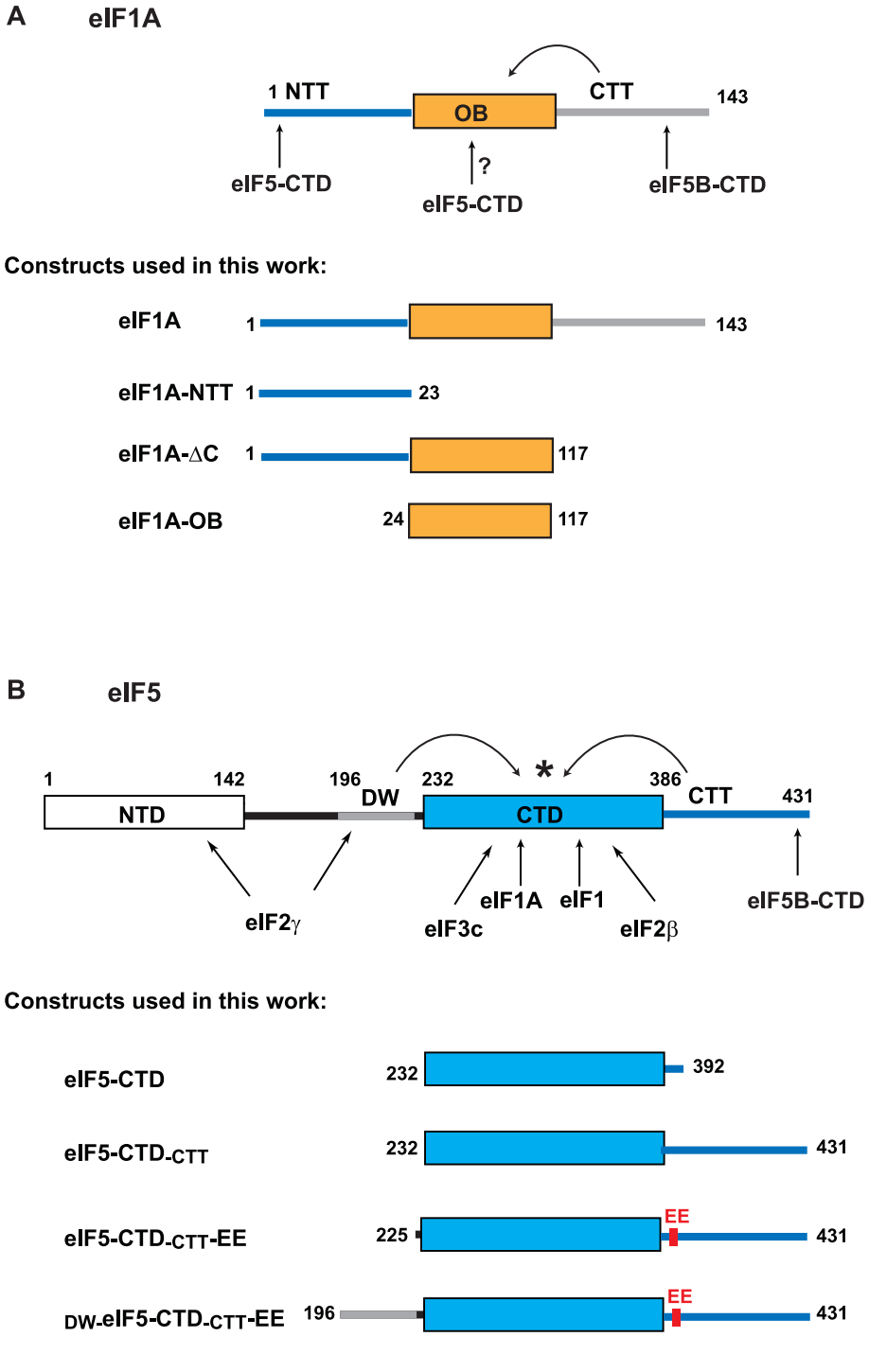


**Fig. 1.** Domain organization of eIF1A and eIF5 and constructs used.
**(A)** *Top*, domain organization of eIF1A. The folded OB domain is shown with a rectangle. The intrinsically disordered N- and C-terminal tails (NTT and CTT, respectively) are shown with lines. Sites of inter- and intra-molecular interactions are shown with arrows. *Bottom*, constructs used in this work. Note that residue numbering in eIF1A does not count the first methionine, which is co-translationally removed *in vivo*. **(B)** *Top*, domain organization of eIF5. The folded domains are shown with rectangles. The intrinsically disordered regions are shown with lines. Sites of inter- and intra-molecular interactions are shown with arrows. The competition between the DWEAR motif and the CTT (Paul et al., 2022) is indicated with a "*". *Bottom*, constructs used in this work. In constructs carrying the phosphomimetic S389E/S390E mutation (labeled with "EE" at the end of the name), the mutation site is marked with a red box labeled "EE". (For interpretation of the references to color in this figure legend, the reader is referred to the Web version of this article.)

mutant of eIF5-CTD (S389E/S390E), mimicking phosphorylation by CK2, further increases the affinity of eIF5-CTD for eIF1A. Our results also suggest possible contact sites of eIF5-CTT and of AA-box 2 on eIF1A.

## 2. Results

### 2.1. eIF5-CTD contacts the OB domain of eIF1A

To determine whether eIF5 contacts eIF1A on its OB domain, we used the NMR chemical shift perturbation (CSP) assay with several eIF5-CTD and eIF1A constructs (the constructs used in this work are shown in Fig. 1). In this assay, spectra of a labeled protein are compared in the presence and absence of an unlabeled binding partner. The NMR experiment used is most often $^{15}$N–$^{1}$H heteronuclear single-quantum coherence (HSQC) on a $^{15}$N-labeled protein, which gives a peak for every NH group in the protein. The peak positions are determined by the chemical shifts of the $^{15}$N and $^{1}$H nuclei of the HN groups, which are highly sensitive to their chemical environment. Therefore, when binding of the invisible partner changes the environment around one of these HN groups, the peak will move, making it possible to map the interactions between the two binding partners on the $^{15}$N-labeled protein. If the dissociation rate of the complex is much faster than the frequency difference in Hz between the NMR chemical shifts (peak positions) in the free and bound state (fast exchange on the NMR time scale), the observed chemical shift is the weighted average of the chemical shifts in the free and bound states; and the peak moves toward the bound state as a function of ligand concentration, which changes the fraction of time the labeled protein spends in the bound state. If the dissociation rate of the complex is comparable to the frequency difference in Hz between the peak positions in the free and bound state (intermediate exchange on the NMR time scale), the NMR peak becomes broadened when only a portion of the labeled protein is bound. When the dissociation rate of the complex

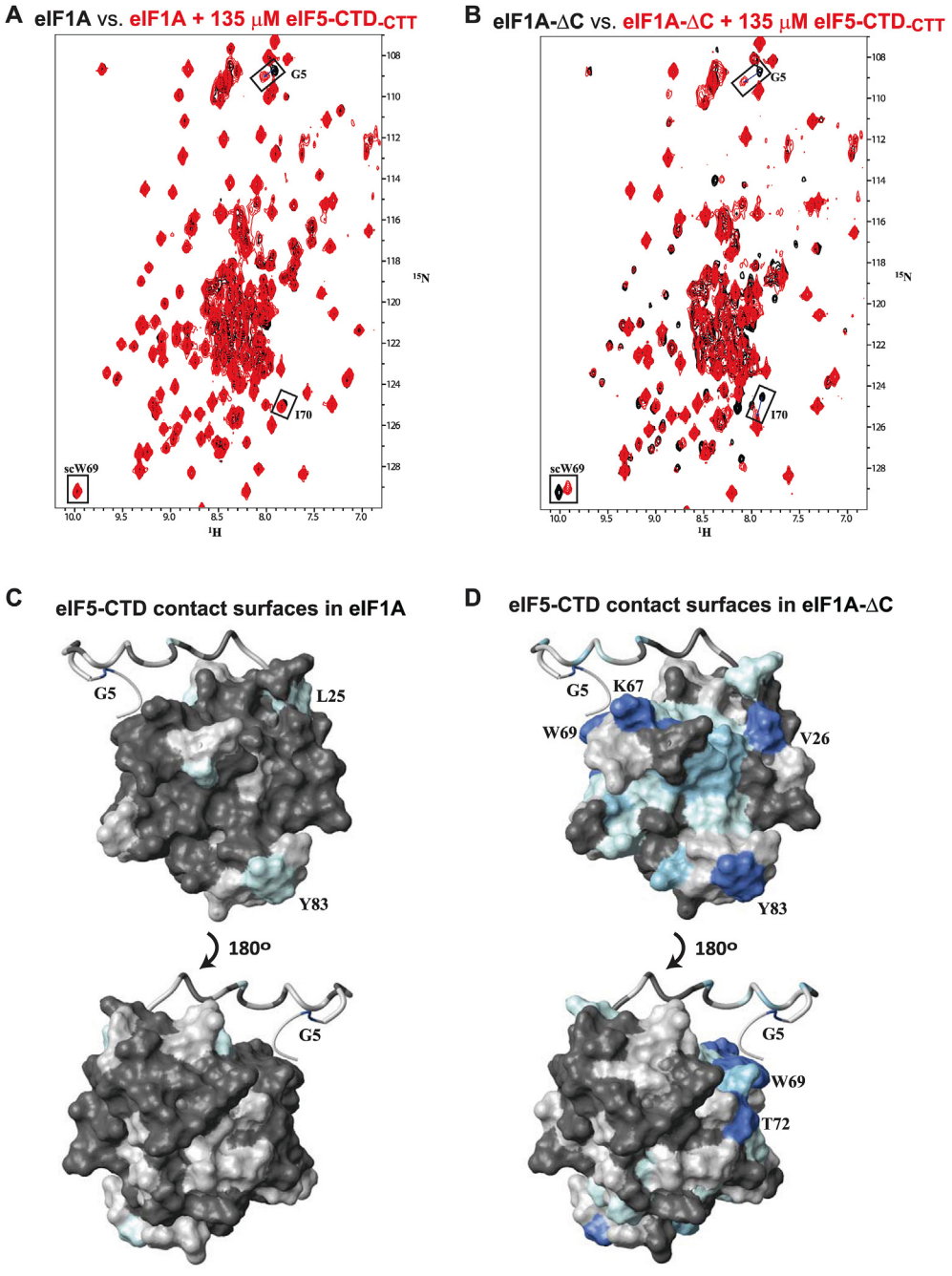


**Fig. 2.** Mapping the CSP effects of eIF5-CTD$_{-CTT}$ on eIF1A
**(A)** Overlay of NMR spectra of 50 μM $^{15}$N/$^{2}$H-labeled eIF1A in the absence (black) and presence of 135 μM unlabeled eIF5-CTD$_{-CTT}$ (red). A few examples of chemical shift perturbation (CSP) effects are marked with black rectangles. **(B)** Overlay of NMR spectra of 50 μM $^{15}$N/$^{2}$H-labeled eIF1A-ΔC in the absence (black) and presence of 135 μM unlabeled eIF5-CTD$_{-CTT}$ (red). **(C)** NMR CSP effects of eIF5-CTD$_{-CTT}$ mapped on the structure of eIF1A. The eIF1A-NTT is shown as a ribbon as it is dynamic in solution. Residues 6–23 (thicker ribbon) are shown in their conformation from the closed 48S PIC (Simonetti et al., 2020). Residues 1–5 (thinner ribbon) remain disordered in the PIC and are modeled in a random conformation for display purposes only. eIF1A-CTT is not shown. Residues with CSP effects are colored from light blue (weak effects) to dark blue (strong effects). Residues that could not be analyzed are light grey. Residues without significant CSP effects are dark grey. Visible residues with stronger CSP effects are labeled. **(D)** NMR CSP effects of eIF5-CTD$_{-CTT}$ on eIF1A-ΔC. Display and coloring are as in panel (C). (For interpretation of the references to color in this figure legend, the reader is referred to the Web version of this article.)

is much slower than the frequency difference in Hz between the peak positions in the free and bound state (slow exchange on the NMR time scale), the free and bound states give rise to separate peaks, whose relative intensities correspond to the fraction of the labeled protein that is bound to the ligand, and change as a function of ligand concentration. In the NMR experiments reported in this work, all the interactions are in fast exchange (peaks moving as a function of ligand concentration). The maximum chemical shift change observed was about 0.2 ppm (~100 Hz on a 500 MHz instrument); therefore, all dissociation rates are faster than 100/s.

NMR experiments are highly sensitive to the size/tumbling rate of the molecule. Slow-tumbling molecules experience line broadening and sometimes complete loss of signal due to transverse relaxation. The signal in a standard $^{1}H–^{15}N$ HSQC experiment quickly deteriorates above 30 kDa, except in dynamic segments that tumble faster than the overall molecule or complex (reviewed in (Marintchev et al., 2007)). eIF5-CTD tends to reversibly self-associate at high protein concentrations and physiological salt (150 mM), The previous characterizations of the eIF5 - eIF1A interactions, done using standard HSQC experiments, were performed at higher salt concentrations to reduce self-association, but the spectra quality was still poor (Luna et al., 2013). Here, we used the Transverse Relaxation Optimized spectroscopy (TROSY) version of $^{15}N–^{1}H$-HSQC experiments with deuterated protein at lower concentrations. The combination of TROSY, which allows observing larger complexes, and lower protein concentration, which reduces self-association, allowed us to obtain higher quality spectra, while using physiological salt (150 mM).

Binding of an unlabeled eIF5 fragment, residues 232–431, which covers the CTD and CTT (eIF5-CTD$_{-CTT}$) to $^{15}N/^{2}H$-labeled eIF1A causes large CSP effects in the eIF1A-NTT and small effects in the eIF1A OB domain (Fig. 2A). Consistent with this observation, in the article reporting that eIF5-CTD contacts the eIF1A-NTT, the NMR spectra of eIF1A in the presence of eIF5-CTD showed not only CSPs in peaks corresponding to the eIF1A-NTT, but also disappearance of the NMR peaks corresponding to the folded OB domain of eIF1A (see Fig. 2B in (Luna et al., 2013)). As described above, loss of signal in peaks corresponding to

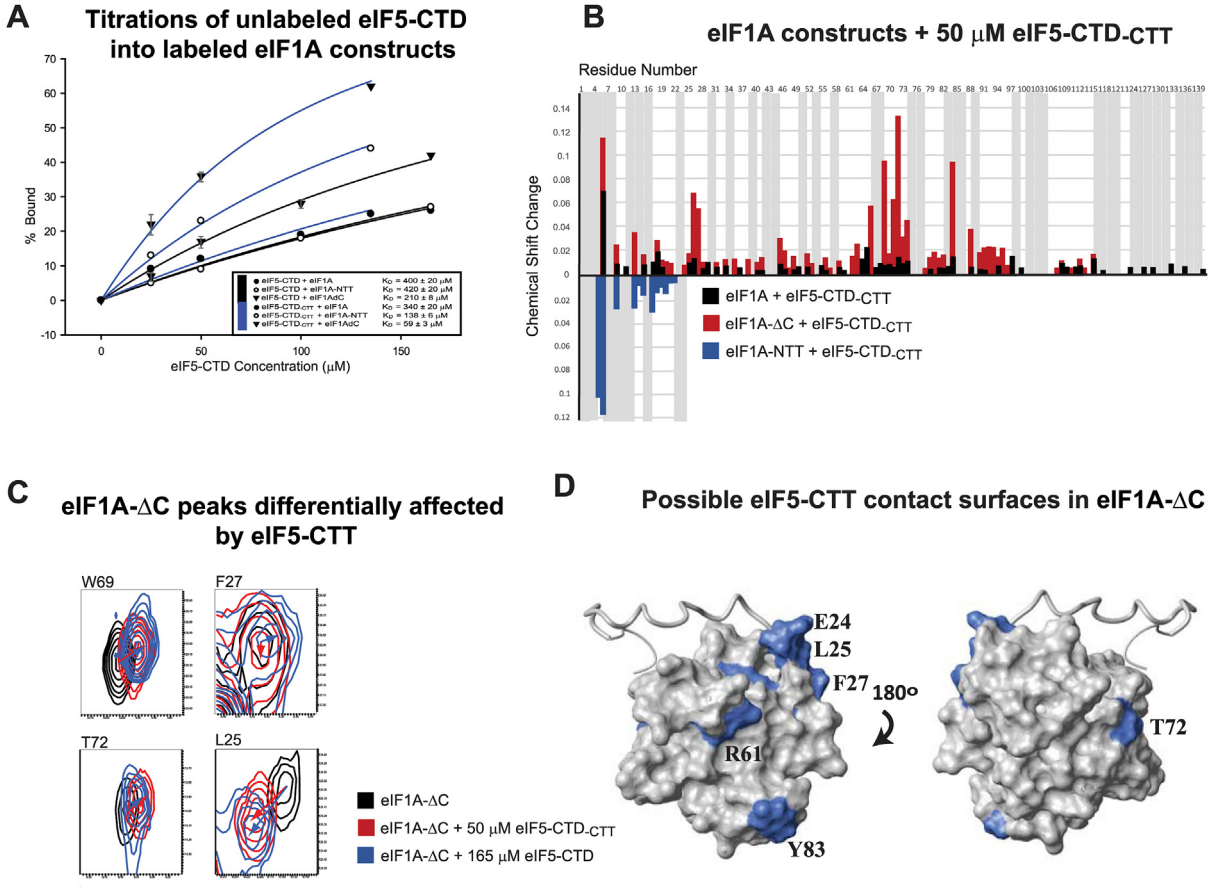


**Fig. 3.** Binding affinities between eIF5-CTD and eIF1A constructs

**(A)** NMR CSP assay titrations of increasing concentrations of unlabeled eIF5-CTD (black lines) and eIF5-CTD$_{-CTT}$ (blue lines) into $^{15}N/^{2}H$-labeled eIF1A (black circles), eIF1A-NTT (clear circles), and eIF1A-ΔC (black triangles). Percent bound of the labeled protein is plotted as a function of the concentration of the unlabeled protein. $K_D$s are shown in the inset. In eIF1A and eIF1A-NTT, fitting was done using the chemical shifts of a single NTT peak (G5). In eIF1A-ΔC, fitting was done using an average of the chemical shifts of several OB domain peaks; standard deviations are shown as grey bars for those data points. Note that the highest concentration data point does not have standard deviation, because the magnitude of CSP was used to normalize the lower concentration points. **(B)** NMR CSP effects of 50 μM eIF5-CTD$_{-CTT}$ on 50 μM $^{15}N/^{2}H$-labeled eIF1A (upward-facing black bars), eIF1A-ΔC (upward-facing red bars) and eIF1A-NTT (downward-facing blue bars). Unanalyzable peaks are shown with grey bars. **(C)** Overlay of NMR spectra of 50 μM $^{15}N/^{2}H$-labeled eIF1A-ΔC in the absence (black) and presence of 50 μM eIF5-CTD$_{-CTT}$ (red), or 165 μM eIF5-CTD (blue) zoomed in to show peaks corresponding to individual residues on the OB domain. Red arrows track the movement of the peaks in presence of eIF5-CTD$_{-CTT}$; blue arrows track the movement of the peaks in presence of eIF5-CTD. The peak corresponding to W69 is representative of how the eIF1A-NTT peaks and most eIF1A OB domain peaks move, the peaks in the presence of eIF5-CTD$_{-CTT}$ and eIF5-CTD moving in the same direction, with the peak in the presence of eIF5-CTD moving slightly more (note the difference in concentrations). The peaks corresponding to F27, T72 and L25 are examples of differential effects of eIF5 with and without the eIF5-CTT, suggesting residues which the eIF5-CTT may be contacting. **(D)** Possible eIF5-CTT contact surfaces mapped on eIF1A-ΔC in blue based on differential CSP effects with and without the eIF5-CTT. Visible residues with differential effects are labeled. (For interpretation of the references to color in this figure legend, the reader is referred to the Web version of this article.)

the OB domain in the HSQC experiment indicates slowing its tumbling rate due to contacts with eIF5-CTD. Most of the contacts on the OB domain are on surfaces known to dynamically contact the eIF1A-CTT (Nag et al., 2016) (Figs. 2C and 3B), notably the region between residues 60 and 90, encompassing helix α1, strand β4, and the surrounding loops (see (Battiste et al., 2000)). This observation suggests possible interference by eIF1A-CTT in the interaction between eIF5-CTD and the OB domain of eIF1A. To explore this possibility, the CSP assay was repeated using eIF1A$_{1\text{-}117}$ (eIF1A-ΔC), which lacks the CTT. The CSP effects on eIF1A-ΔC were consistently stronger throughout the protein (Fig. 2BD, 3B), but particularly so in the OB domain, supporting the hypothesis that eIF1A-CTT interferes with the ability of eIF5-CTD to bind to this surface. The CSP assay was repeated with eIF1A$_{24\text{-}117}$ (eIF1A-OB), a construct of eIF1A that consists of only the OB domain and lacks both the NTT and CTT, to test whether the OB domain could bind to eIF5-CTD in the absence of the NTT. The effects of eIF5-CTD on eIF1A-OB were qualitatively similar to those on eIF1A-ΔC, but weaker; however, the quality of the spectra was poor, due to the limited solubility and stability of eIF1A-OB (data not shown). Therefore, while the OB domain can bind to eIF5-CTD on its own, the NTT appears to stabilize the interaction.

We used NMR titration with a set of $^{15}N/^{2}H$-labeled eIF1A constructs to determine their affinities for eIF5-CTD$_{\text{-CTT}}$ and eIF5-CTD (residues 232–392, encompassing the folded domain plus the first few residues of the eIF5-CTT, which are part of AA-box 2). Thus, both eIF5-CTD constructs include the entire AA-box 2. The additional contacts in eIF1A-ΔC mediated by the OB domain appear to contribute modestly to the overall affinity (Fig. 3A), with roughly two-fold increase in affinity for eIF5-CTD$_{\text{-CTT}}$ ($K_D$ = 59 μM), when compared to its affinity for 1A-NTT alone ($K_D$ = 138 μM). The full-length eIF1A, however, was observed to have significantly lower affinity for eIF5-CTD$_{\text{-CTT}}$ ($K_D$ = 340 μM), indicating that the presence and dynamic contacts of the eIF1A-CTT could also be interfering with the interaction between eIF1A-NTT and eIF5-CTD. This interpretation is supported by the greater magnitude of effects on the NTT residues in both eIF1A-ΔC and eIF1A-NTT, compared to the full length eIF1A (Fig. 3B). eIF5-CTD has about three-fold lower affinity for eIF1A-ΔC ($K_D$ = 210 μM) and eIF1A-NTT ($K_D$ = 420 μM) than eIF5-CTD$_{\text{CTT}}$ (Fig. 3A), which indicates that eIF5-CTT contributes to the interaction between eIF5 and eIF1A, and contacts eIF1A-NTT, because eIF5-CTD$_{\text{-CTT}}$ has higher affinity for eIF1A-NTT than does eIF5-CTD. However, eIF5-CTD and eIF5-CTD$_{\text{-CTT}}$ had similar affinities for full-length eIF1A ($K_D$s of 400 μM and 340 μM, respectively), suggesting that the negatively charged eIF1A-CTT interferes with binding of eIF5-CTT, which is also negatively charged. Furthermore, when comparing the spectra of labeled eIF1A-ΔC with eIF5-CTD and eIF5-CTD$_{\text{-CTT}}$, there were differential CSP effects on multiple residues in the OB domain (Fig. 3CD), not only near the NTT (E24, L25, and F27), but also elsewhere on the OB surface (R61, T72, Y83, Y94), suggesting that the eIF5-CTT could also be contacting the OB domain at these surfaces, in addition to contacting eIF1A-NTT.

### 2.2. The S389E/S390E phosphomimetic mutation in eIF5-CTD increases its affinity for eIF1A

eIF5 is phosphorylated by CK2 at S389/S390 in acidic/aromatic box 2 (AA-box 2) (Homma et al., 2005). We had previously observed that introducing a phosphomimetic mutation (S389E/S390E) at these positions significantly increases the affinity of eIF5 for eIF2β (Paul et al., 2022). Given that the eIF1A binding site on eIF5-CTD has significant overlap with that of eIF2β, including the AA-box 2, it was possible that phosphorylation of eIF5 by CK2 could also modulate its affinity for eIF1A. As hypothesized, the phosphomimetic mutant, eIF5-CTD$_{\text{-CTT}}$-EE, led to a large increase in CSP effects in the eIF1A constructs when compared to its wild-type (WT) counterpart (Fig. 4), suggesting that phosphorylation by CK2 stabilizes the interaction between these two proteins. In spectra of labeled eIF1A-ΔC, at higher concentrations of eIF5-CTD$_{\text{-CTT}}$-EE, it was observed that the peak corresponding to G5 in the eIF1A-NTT begins to broaden and decrease in intensity and completely disappears at 100 μM eIF5-CTD (data not shown), indicating the possibility of conformational exchange. No evidence of such conformational exchange was apparent in spectra of eIF1A-NTT, indicating that the effect could possibly be due to eIF1A-NTT and -OB being in proximity to each other on the surface of eIF5-CTD, which would lead to the NTT experiencing different environments as the OB domain is dynamically binding and dissociating from the eIF5-CTD surface.

The affinity of eIF5-CTD$_{\text{-CTT}}$-EE for all the eIF1A constructs was higher than that of the wild type eIF5-CTD$_{\text{-CTT}}$ (Fig. 5A). Among the eIF1A constructs, the relative affinities for eIF5-CTD$_{\text{-CTT}}$-EE stayed similar to those for WT eIF5-CTD$_{\text{-CTT}}$, with eIF1A-ΔC having a three-fold higher affinity ($K_D$ = 15 μM) than eIF1A-NTT ($K_D$ = 45 μM), which in turn, had three-fold higher affinity than full length eIF1A ($K_D$ = 147 μM), further supporting the evidence that the eIF1A-CTT interferes with eIF5-CTD binding.

While the C-terminal, intrinsically disordered segment of AA-box 2 around the mutated residues likely contacts eIF1A-NTT (because the mutant, eIF5-CTD$_{\text{-CTT}}$-EE has three-fold higher affinity for eIF1A-NTT ($K_D$ = 45 μM) than does WT eIF5-CTD$_{\text{-CTT}}$ ($K_D$ = 138 μM) (Fig. 5A)), the eIF5-CTT could also be contacting the OB domain. The possible contact surfaces for the mutated residues in eIF5-CTD can be observed by comparing CSP effects on eIF1A-ΔC caused by WT and mutant eIF5-CTD. While the CSP effects in the presence of the mutant are stronger throughout the protein (Fig. 5C), the magnitude of the changes is different in some areas. Note that we compared 50 μM concentration of eIF5-CTD$_{\text{-CTT}}$-EE to 135 μM concentration of WT eIF5-CTD$_{\text{-CTT}}$. At these concentrations, the percent eIF1A-ΔC bound is almost the same, slightly higher with the WT eIF5-CTD$_{\text{-CTT}}$ (Fig. 5A). This pattern was observed in most of the affected peaks in the eIF1A-ΔC spectra. In contrast, residues R61, L64, W69, and T72 showed smaller than expected effect, and L25, V26, Y83, and Y94 showed greater than expected effect (Fig. 5B), indicating a possible area on eIF1A-OB, contacted by the C-terminal portion of AA-box 2. These effects could not be seen on full length eIF1A, consistent with eIF1A-CTT interfering with this potential binding site.

### 2.3. eIF1A-NTT and -OB domain contact distinct but overlapping surfaces in eIF5-CTD

We used CSP assays with labeled eIF5-CTD$_{\text{-CTT}}$-EE and different eIF1A constructs to map their respective contact surfaces on eIF5-CTD$_{\text{-CTT}}$ (Fig. 6). In these assays, eIF1A had stronger effects than previously observed with WT eIF5-CTD; and eIF1A-ΔC caused even stronger CSP effects on eIF5-CTD$_{\text{-CTT}}$-EE, as expected from its higher affinity. The spectrum quality, however, was poorer than with full-length eIF1A or eIF1A-NTT, possibly due to the larger effective size of the complex (and slower tumbling) when the eIF1A OB domain is bound to eIF5-CTD (data not shown). eIF1A-NTT and eIF1A-OB binding affected distinct but overlapping surfaces (Fig. 6BC). The former had stronger CSP effects, when added at the same concentration. The main eIF1A-NTT contact surfaces involve AA box 1 (the C-terminal portion of helix α8, the N-terminal portion of helix α9, and the connecting loop), and AA-box 2 (the C-terminal portion of helix α10 and the following loop (Bieniossek et al., 2006). In contrast, the OB domain predominantly contacts the N-terminal portion of helix α8, the C-terminal portion of helix α9, the N-terminal portion of helix α10, and the connecting loop between them (Fig. 6BC). The eIF1A-OB domain contact surface on eIF5-CTD overlaps partially with the intramolecular contact surface for the DWEAR motif (Paul et al., 2022). We had previously observed weak CSP effects there from eIF1A binding to WT eIF5-CTD and eIF5-CTD$_{\text{-CTT}}$, but not to the longer $_{\text{DW}}$eIF5-CTD$_{\text{-CTT}}$ construct that also included the DWEAR motif (Paul et al., 2022). Accordingly, we did not observe these CSP effects when we added unlabeled eIF1A-ΔC to the longer $_{\text{DW}}$eIF5-CTD$_{\text{-CTT}}$-EE mutant, which also contains the DWEAR motif. The spectra quality was better than with eIF5-CTD$_{\text{-CTT}}$-EE (data not shown), also consistent with the DWEAR motif interfering with the eIF1A-OB domain contacts.

To further explore the interplay between eIF1A-NTT and -OB domain

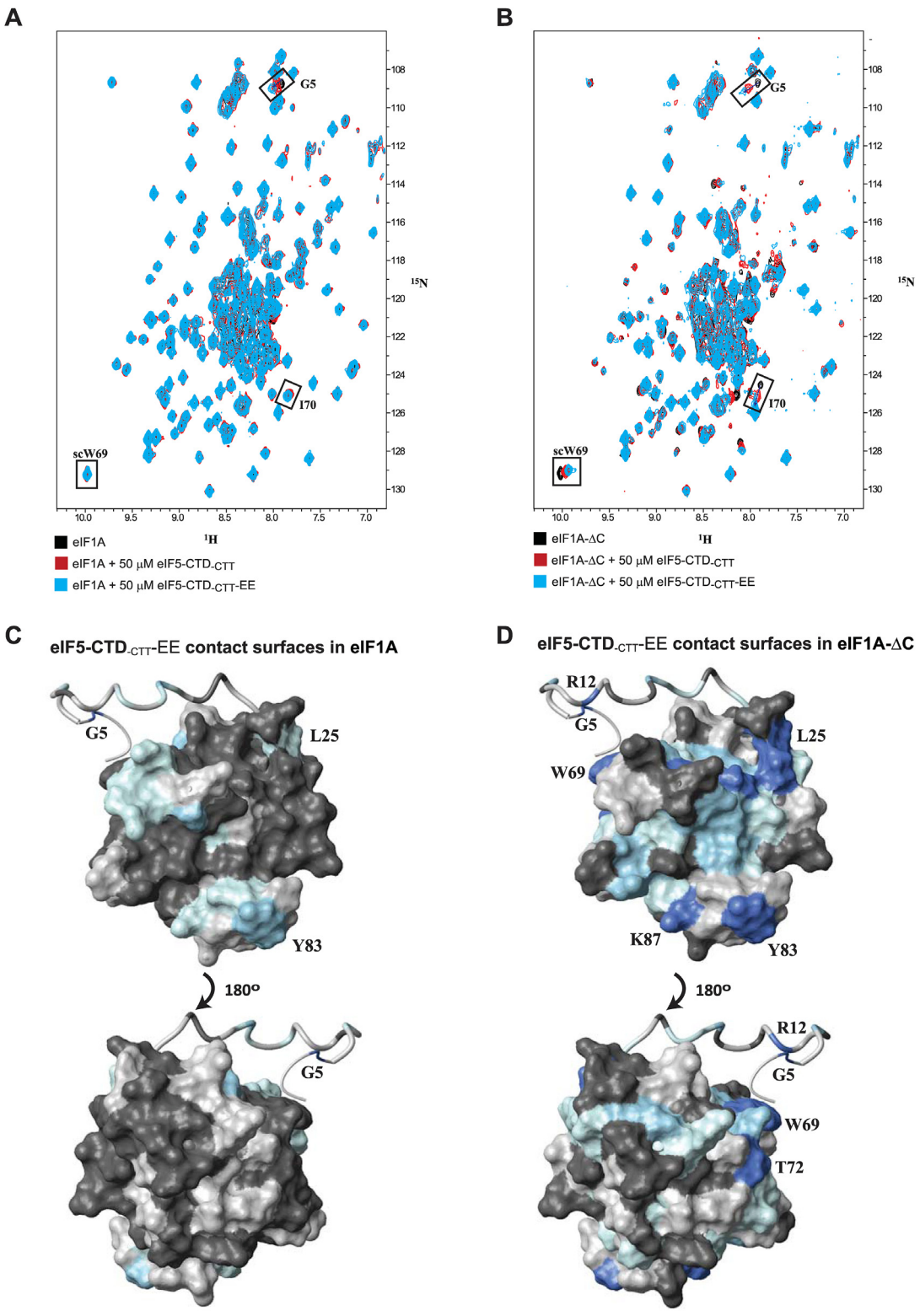


**Fig. 4.** Effects of the eIF5-CTD S389E/S390E phosphomimetic mutation on binding to eIF1A
**(A)** Overlay of NMR spectra of 50 μM $^{15}N/^{2}H$-labeled eIF1A in the absence (black) and presence of 50 μM unlabeled eIF5-CTD$_{-CTT}$ (red), or 50 μM unlabeled eIF5-CTD$_{-CTT}$-EE (blue). A few examples of chemical shift perturbation (CSP) effects are marked with black rectangles. **(B)** Overlay of NMR spectra of 50 μM $^{15}N/^{2}H$-labeled eIF1A-ΔC in the absence (black) and presence of 50 μM unlabeled eIF5-CTD$_{-CTT}$ (red), or 50 μM unlabeled eIF5-CTD$_{-CTT}$-EE (blue). **(C)** NMR CSP effects of eIF5-CTD$_{-CTT}$-EE on eIF1A. The eIF1A-NTT is shown as a ribbon as it is dynamic in solution. Residues 6–23 (thicker ribbon) are shown in their conformation from the closed 48S PIC (Simonetti et al., 2020). Residues 1–5 (thinner ribbon) remain disordered in the PIC and are modeled in a random conformation for display purposes only. eIF1A-CTT is not shown. Residues with CSP effects are colored from light blue (weak effects) to dark blue (strong effects). Residues that could not be analyzed are light grey. Residues without significant CSP effects are dark grey. Visible residues with strong CSP effects are labeled. **(D)** NMR CSP effects of eIF5-CTD$_{-CTT}$-EE on eIF1A-ΔC. Display and coloring are as in panel (C). (For interpretation of the references to color in this figure legend, the reader is referred to the Web version of this article.)

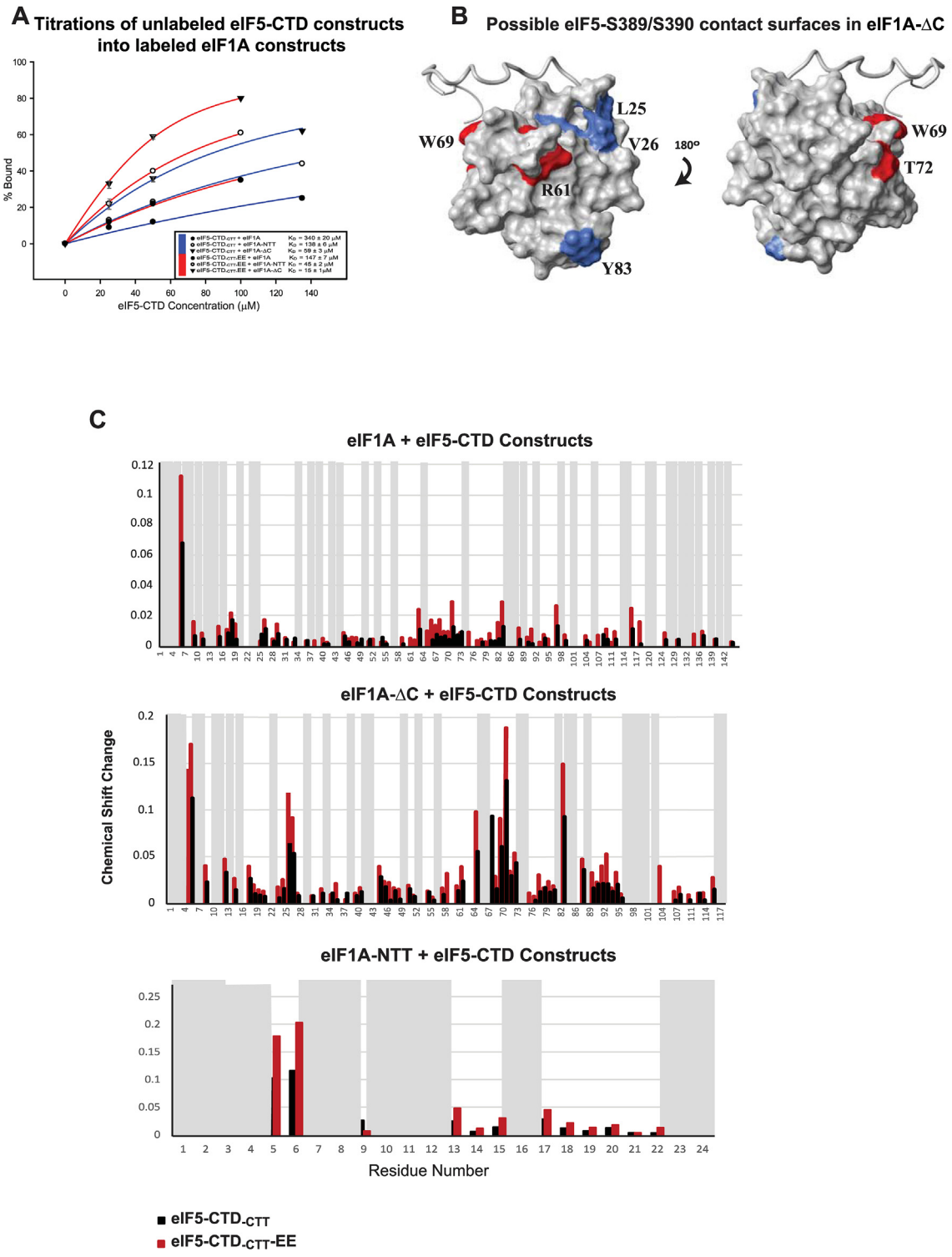


**Fig. 5.** Effect of the eIF5-CTD S389E/S390E phosphomimetic mutation on the affinity for eIF1A
**(A)** NMR chemical shift perturbation (CSP) assay titrations of increasing concentrations of unlabeled eIF5-CTD$_{-CTT}$ (blue lines) and eIF5-CTD$_{-CTT}$-EE (red lines) into 50 μM $^{15}$N/$^{2}$H-labeled eIF1A (black circles), eIF1A-NTT (clear circles), and eIF1A-ΔC (black triangles). Percent bound of the labeled protein is plotted as a function of the concentration of the unlabeled protein. $K_D$s are shown in the inset. In eIF1A and eIF1A-NTT, fitting was done using the chemical shifts of a single NTT peak (G5). In eIF1A-ΔC, fitting was done using an average of the chemical shifts of several OB domain peaks; standard deviations are shown as grey bars for those data points. Note that the highest concentration data point does not have standard deviation, because the magnitude of CSP was used to normalize the lower concentration points. **(B)** Possible contact surfaces for the segment around the eIF5-CTD S389E/S390E phosphomimetic mutation site on the eIF1A OB domain, mapped on eIF1A. Residues colored in blue (L25, V26, Y83, Y94) have greater than average difference in CSP effects between eIF5-CTD$_{-CTT}$-EE and eIF5-CTD$_{-CTT}$. Residues colored red (R61, L64, W69, T72) have smaller than average difference in CSP effects. Visible residues with differential effects are labeled. **(C)** NMR CSP effects of 50 μM eIF5-CTD$_{-CTT}$ (black bars) and eIF5-CTD$_{-CTT}$-EE (red bars) on 50 μM $^{15}$N/$^{2}$H-labeled eIF1A (top), eIF1A-ΔC (middle), and eIF1A-NTT (bottom). Unanalyzable peaks are shown with grey bars. (For interpretation of the references to color in this figure legend, the reader is referred to the Web version of this article.)

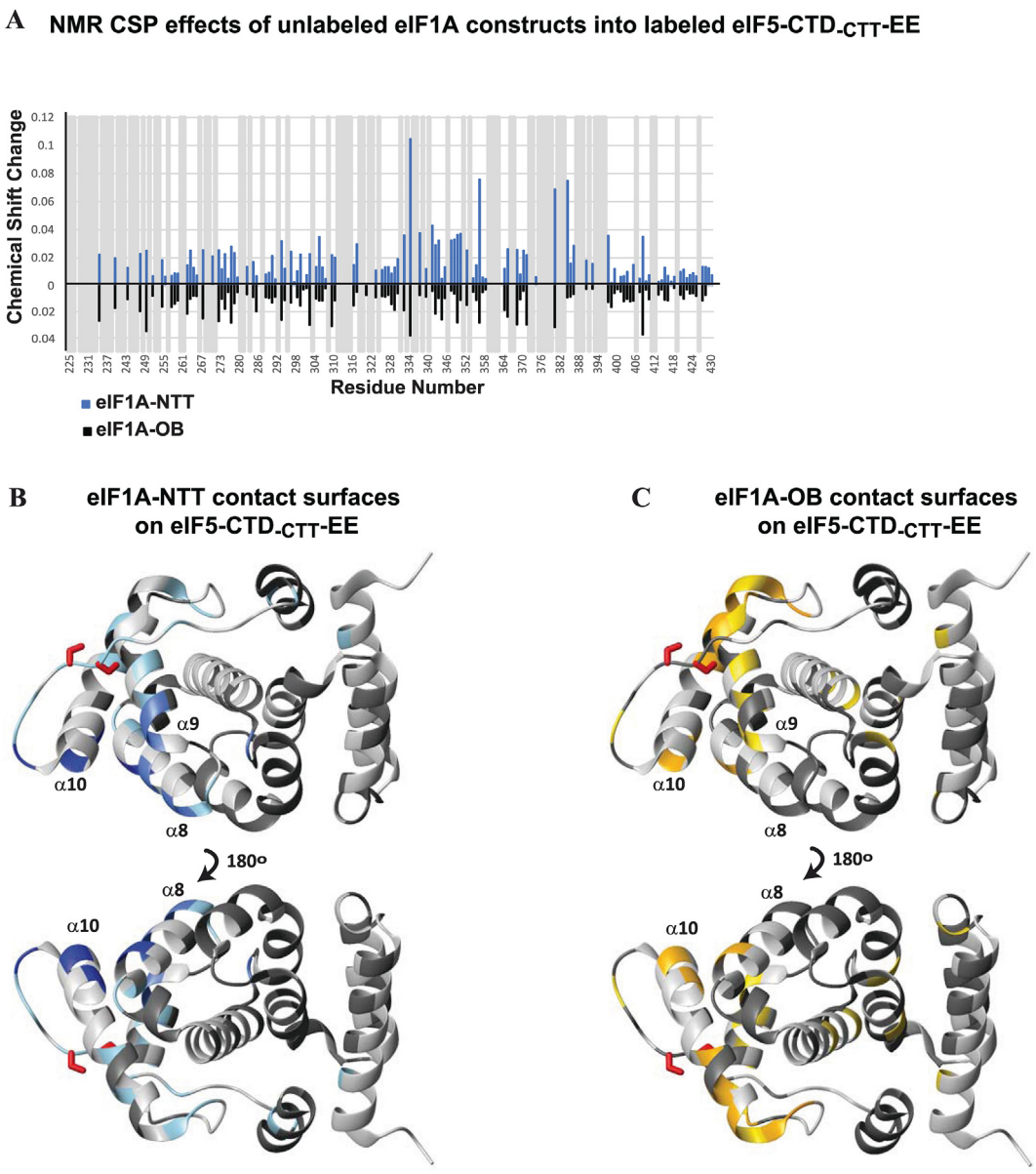


**Fig. 6.** Mapping the eIF1A contact surfaces on eIF5-CTD$_{-CTT}$-EE
**(A)** NMR CSP effects of 100 μM eIF1A-NTT (blue bars) and eIF1A-OB (black bars) on 50 μM $^{15}N/^{2}H$-labeled eIF5-CTD$_{-CTT}$-EE. Unanalyzable peaks are shown with grey bars. **(B)** eIF1A-NTT contact surfaces on eIF5-CTD$_{-CTT}$-EE. Residues with CSP effects are colored from light blue (weak effects) to dark blue (strong effects). Residues that could not be analyzed are light grey. Residues without significant CSP effects are dark grey. The side chains of the mutated residues S389 and S390 are shown as sticks and colored red. Helices α8, α9, and α10 are labeled. The human eIF5-CTD structure and the numbering of helices is from (Bieniossek et al., 2006). **(C)** eIF1A-OB contact surfaces on eIF5-CTD$_{-CTT}$-EE. Residues with CSP effects are colored from gold (weak effects) to orange (strong effects). The rest is as in panel (B). (For interpretation of the references to color in this figure legend, the reader is referred to the Web version of this article.)

in eIF5-CTD binding, we performed a competition assay using NMR CSP. In this assay, we compared the CSP effects of 50 μM mutant eIF5-CTD$_{-CTT}$-EE on labeled eIF1A-ΔC in the presence and absence of a higher (150 μM) concentration of eIF1A-NTT. In the presence of both the eIF5-CTD mutant and eIF1A-NTT, the CSP effects were reduced throughout eIF1A-ΔC; however, the decrease was not proportional (Table 1). The effects were reduced the most in the NTT of eIF1A-ΔC (>30% reduction), showing competition with the free NTT. The CSP effects were reduced less in the OB domain peaks, where the reduction was 25% or less. The reduction of only ~35% in binding of the NTT portion of eIF1A-ΔC in the presence of 3-fold excess of eIF1A-NTT is consistent with eIF1A-ΔC having three-fold higher affinity than free eIF1A-NTT (Fig. 5A). The reduced binding of the OB domain is likely due to weakening of OB binding in the absence of the NTT interaction (if the presence of the OB domain stabilizes the NTT interaction, then the NTT interaction stabilizes the OB interaction as well). However, some direct effects of the NTT on the eIF1A-OB binding cannot be excluded, and could help explain the varying degrees of inhibition on different eIF1A-OB domain surfaces.

To directly assess the interplay between eIF1A and eIF2β-NTT in eIF5-CTD binding, we performed a competition assay similar to the one above. In this assay, we compared the CSP effects of 50 μM mutant eIF5-CTD$_{-CTT}$-EE on labeled eIF1A-ΔC in the presence and absence of 100 μM eIF2β-NTT. In the presence of both the eIF5-CTD mutant and eIF2β-NTT, the CSP effects in the NTT of eIF1A-ΔC were nearly completely abolished (>83% reduction), showing competition between eIF1A-NTT and eIF2β-NTT (Table 1, Fig. S1). In contrast, the reduction of CSP effects was much smaller in the OB domain peaks, 63% or less. Thus, eIF2β-NTT competes with the eIF1A-NTT, but not -OB domain, for binding to eIF5-CTD. The

**Table 1**
Reduction of NMR CSP effects upon adding excess unlabeled eIF1A-NTT or eIF2β-NTT to a complex of $^{15}N/^{2}H$-labeled eIF1A-ΔC and unlabeled eIF5-CTD$_{-CTT}$-EE.

| eIF1A-ΔC Residue | % CSP Reduction | |
|---|---|---|
| | eIF1A-NTT 150 μM | eIF2β-NTT 100 μM |
| G5 | 40% | 95% |
| E17 | 32% | 83% |
| **NTT average** | **36 ± 4%** | **89 ± 6%** |
| L25 | 20% | 62% |
| V26 | 24% | 38% |
| W69 | 22% | 63% |
| Y83 | 18% | N/A |
| **OB average** | **21 ± 2%** | **50 ± 10%** |

Percent reduction in CSP effects on 50 μM $^{15}N/^{2}H$-labeled eIF1A-ΔC in the presence of 50 μM unlabeled eIF5-CTD$_{-CTT}$ EE upon addition of 150 μM unlabeled eIF1A-NTT or 100 μM unlabeled eIF2β-NTT. eIF1A-NTT residues G5 and E17, and OB domain residues E25, V26, W69, and Y83 were used for the analysis. Values are rounded to the last significant digit. N/A, not analyzable.

effect of 100 μM eIF2β-NTT is greater than that of 150 μM eIF1A-NTT, consistent with its higher affinity and up to three binding sites for eIF5-CTD (Paul et al., 2022). As above, the reduced binding of the OB domain is likely indirect, due to weakening of OB binding in the absence of the NTT interaction.

## 3. Discussion

eIF1A is known to interact with eIF5 through its N-terminus (Luna et al., 2013). Here we show that eIF5 also contacts the OB domain. The contact surface on the eIF1A-OB domain showed significant overlap with the previously mapped intramolecular interface with eIF1A-CTT (Nag et al., 2016), indicating that eIF1A-CTT interferes with this interaction (Fig. 2). Indeed, eIF5-CTD$_{-CTT}$ has more than five-fold higher affinity for eIF1A-ΔC than for full length eIF1A (Fig. 3A). The eIF1A-OB domain can bind eIF5-CTD on its own, although with lower affinity than eIF1A-NTT. These additional contacts also contribute to the overall affinity of the interaction, with eIF1A-ΔC having two-fold higher affinity than eIF1A-NTT for both eIF5-CTD and eIF5-CTD$_{-CTT}$ (Fig. 3A). In the absence of eIF1A-CTT, eIF5-CTT appears to also contribute to the eIF5-CTD binding to eIF1A, because eIF5-CTD$_{-CTT}$ has ~3-fold higher affinity for eIF1A-ΔC and eIF1A-NTT than does eIF5-CTD, but the difference is minimal for full-length eIF1A (Fig. 3A). The competition between eIF5-CTT and eIF1A-CTT is not surprising, because both are predominantly negatively charged and could interact with the positively charged eIF1A-NTT as well as positively charged surfaces on the eIF1A-OB domain. It is interesting to note that in *Metazoa* and some fungi, the extreme C-termini of eIF5-CTT and eIF1A-CTT compete for binding to eIF5B (Lin et al., 2018). The difference in affinity of eIF5-CTD$_{-CTT}$ and eIF5-CTD for eIF1A-NTT indicates that eIF5-CTT interacts productively with eIF1A-NTT. When comparing NMR CSP effects of eIF5-CTD and eIF5-CTD$_{-CTT}$ on eIF1A-ΔC, we saw differing effects on OB domain surfaces (Fig. 3CD), suggesting that eIF5-CTT may also contact the OB domain at these surfaces.

eIF5 is phosphorylated by CK2 at S389 and S390 in AA-box 2, which stimulates protein synthesis and cell division (Homma et al., 2005). We previously showed that introducing a phosphomimetic mutation at the site of CK2 phosphorylation (S389E/S390E) significantly increases the affinity of eIF5-CTD for eIF2β, especially in the absence of the DWEAR motif (Paul et al., 2022). Knowing that the binding site of eIF1A on eIF5 largely overlaps with that of eIF2β, including AA-box 2 (Paul et al., 2022), we set out to test whether CK2 phosphorylation could also modulate the affinity of eIF5 for eIF1A, using the same phosphomimetic mutant of eIF5-CTD. Our data showed that the introduction of the phosphomimetic mutation did in fact lead to increase in affinity for the eIF1A constructs with a ~2-fold lower $K_D$ for eIF1A (147 μM), ~3-fold lower $K_D$ for eIF1A-NTT (45 μM), and ~4 fold lower $K_D$ for eIF1A-ΔC (15 μM), compared to the WT eIF5-CTD$_{-CTT}$. Remarkably, eIF5-CTD$_{-CTT}$-EE phosphomimetic mutant has ten-fold higher affinity for eIF1A-ΔC than for full length eIF1A (Fig. 5A). Through differential NMR CSP effects, a potential site of interaction for the eIF5 mutant on the eIF1A OB domain was also observed (Fig. 5BC).

The newly identified eIF1A-OB domain contact surface on eIF5-CTD overlaps partially with the eIF1A-NTT contact surface (Figs. 6 and 7A), as well as with the intramolecular contact surface for the DWEAR motif (Paul et al., 2022). Weak CSP effects are observed there from eIF1A binding to WT eIF5-CTD and eIF5-CTD$_{-CTT}$, but not the longer $_{DW}$eIF5-CTD$_{-CTT}$ construct that also includes the DWEAR motif (Paul et al., 2022), or even with the mutant $_{DW}$eIF5-CTD$_{-CTT}$-EE (this work). Therefore, it appears that efficient eIF1A-OB binding would require both the eIF1A-CTT to be displaced from the eIF1A-OB domain surface and the DWEAR motif to be displaced from the eIF5-CTD surface.

The finding that eIF5-CTD binds to the OB domain of eIF1A raises some intriguing questions. The contact interface overlaps not only with the dynamic intramolecular interface with eIF1A-CTT (Nag et al., 2016), but also with the binding surface for the small ribosomal subunit (Hashem et al., 2013; Lomakin and Steitz, 2013; Weisser et al., 2013; Yu et al., 2009) (Fig. 7B). Therefore, on the ribosome, most of the eIF5-CTD – eIF1A-OB contacts reported here would not be possible, making it unclear at what stage this interaction would take place. The relevant eIF5-containing PICs are the 43S, the open, scanning 48S, and the closed 48S with eIF5-NTD having replaced eIF1. eIF5-CTD should be able to access the eIF1A-NTT, most of which remains dynamic in the 43S PIC and the open 48S PIC (Aylett et al., 2015; Erzberger et al., 2014; Kratzat et al., 2021; Llacer et al., 2015, 2021; Simonetti et al., 2020), and possibly in the closed 48S PIC, where the majority of the eIF1A-NTT is resolved, but the main binding site, near the N-terminus remains exposed and/or disordered, at least in the structure of the mammalian complex (Simonetti et al., 2020) (Fig. 7B), although in yeast closed 48S complexes, the eIF1A N-terminus appears buried (Hussain et al., 2014; Llacer et al., 2015, 2018, 2021). The position of eIF5-CTD within the PIC is unknown at any stage of initiation. The interaction of eIF5-CTD with eIF1 was mapped previously to the eIF1 surface distal from eIF1A (Luna et al., 2012) (Fig. 7B). While if extended, eIF1A-NTT could reach eIF5-CTD as docked on eIF1 in (Luna et al., 2012), this is inconsistent with the position of eIF1A-NTT in PIC structures (Fig. 7B). Furthermore, that surface of eIF1 contacts eIF2γ and eIF3c in the scanning PIC (Fig. 7B), and at least the contact interface with eIF2γ would be incompatible with eIF5-CTD binding there. Instead, the inability to observe eIF5-CTD in PIC structures, at least until now, suggests that it is dynamic and interacting only with mobile segments of PIC components. Those could be the N-terminal region of eIF3c, the N-terminus of eIF1A and/or eIF2β-NTT, but possibly not eIF1A-OB or eIF1 (unless eIF1 stays loosely associated with the closed PIC through contacts with eIF3c and eIF5-CTD).

Thus, there seem to be two binding interfaces involving eIF5-CTD: with eIF1 (Luna et al., 2012), and with eIF1A-OB (this work), which are unlikely to occur within the PIC. The eIF5-CTD•eIF1 interaction could exist within the MFC. But what about the interaction with eIF1A, which is not known to be part of the MFC? If the binding affinity of phosphorylated eIF5 for eIF1A is strong enough, that would introduce the possibility that eIF1A could be part of the multifactor complex (MFC) at least when eIF5 is phosphorylated. This scenario would require the competing intra- and inter-molecular interactions to be disrupted within the MFC: the contacts between eIF1A-CTT and the rest of eIF1A, between the eIF5 DWEAR motif and eIF5-CTD, and/or between eIF2β-NTT and eIF5-CTD. The 15 μM affinity of the phosphomimetic mutant of eIF5-CTD for eIF1A-ΔC is particularly of note as it is approaching physiological concentrations of the protein. Thus, if eIF1A-CTT is disengaged from the OB domain, eIF5 and eIF1A could interact with each other in solution, at least if brought together by common binding partners.

The observation that phosphorylation of eIF5 by CK2 stimulates two competing interactions, with both eIF2β-NTT and eIF1A, raises some

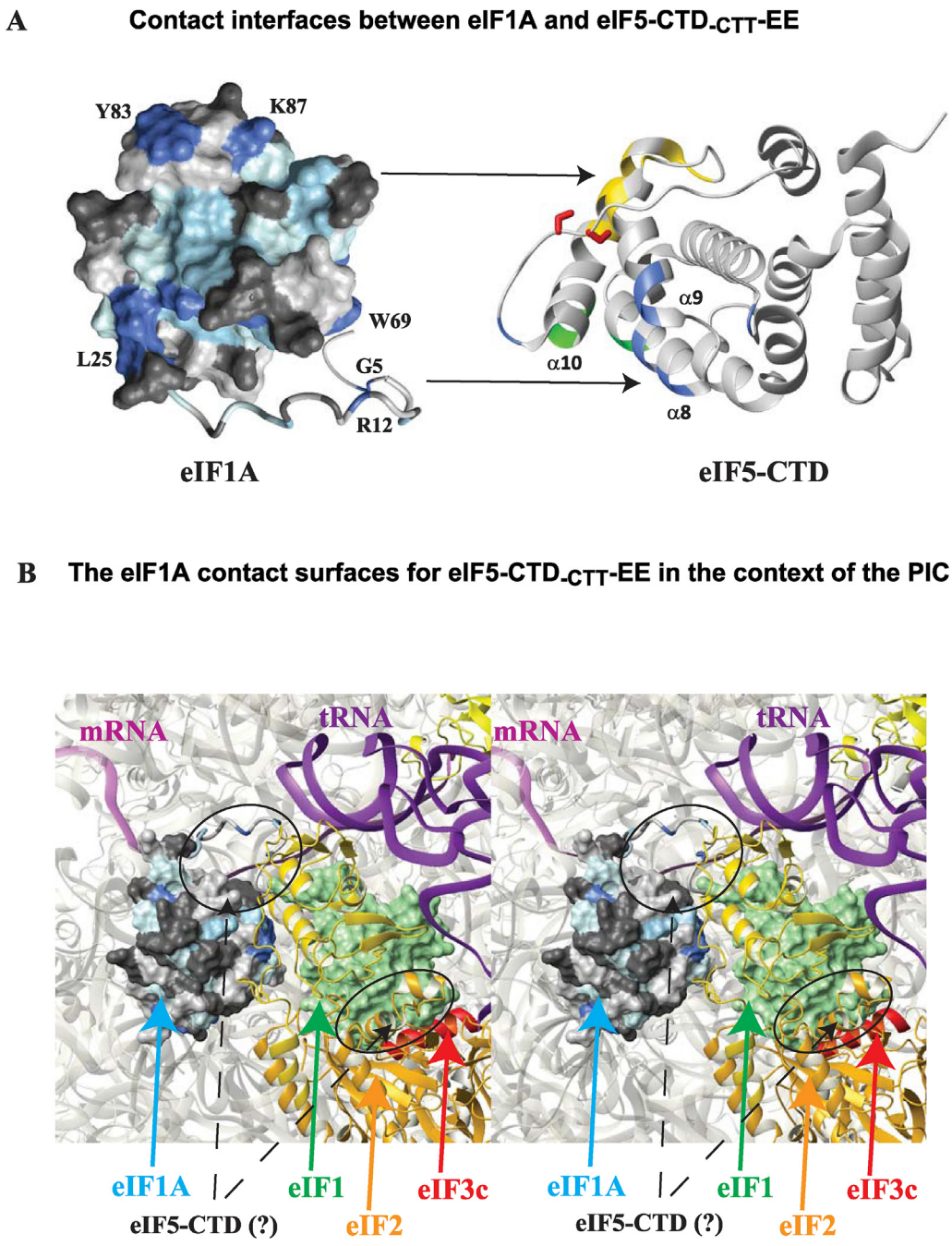


**Fig. 7.** Contact interfaces between eIF1A and eIF5-CTD$_{-CTT}$-EE
**(A)** Contact interfaces between eIF1A-ΔC and eIF5-CTD$_{-CTT}$-EE. Coloring of eIF1A-ΔC is as in Fig. 4D (effects of eIF5-CTD$_{-CTT}$-EE binding to eIF1A-ΔC). The same surface is shown as in the top panel of Fig. 4D, but the image is rotated 180°. Visible residues with strong CSP effects are labeled. eIF5-CTD is in the same orientation as in the top panels of Fig. 6B and *C*. Helices α8, α9, and α10 are labeled. Residues experiencing medium and large CSP effects upon addition of eIF1A-NTT are colored in royal blue. Residues experiencing medium and large CSP effects upon addition of eIF1A-OB are colored in gold. Residues experiencing medium and large CSP effects upon addition of both eIF1A-NTT and eIF1A-OB are colored in green (note that, to focus on the main contact interfaces, smaller CSP effects are ignored). **(B)** Cross-eye stereo view of eIF1A within the 48S PIC, 7qp6.pdb (Yi et al., 2022). eIF1A is colored and displayed as in Fig. 4D and its orientation is similar to that in the bottom panel of Fig. 4D, thus the view is roughly from the opposite side, compared to panel (A), where the visible surface of eIF1A is that from the top panel of Fig. 4D. The eIF1A-OB domain is shown in surface representation. The eIF1A-NTT (not observed in 7qp6.pdb (Yi et al., 2022) is shown as a ribbon. Residues 6–23 are shown in their conformation from the closed 48S PIC structure, 6yal.pdb (Simonetti et al., 2020). Residues 1–5, which remain disordered in all available PIC structures, are modeled in a random conformation for display purposes only. eIF1A-CTT, which remains disordered in the PIC, is not shown. eIF1 (green) is shown in surface representation. eIF2α, β, and γ are shown as yellow, gold, and orange ribbon, respectively. The eIF1-binding helix of eIF3c is red. The mRNA is violet, and the initiator tRNA is purple. The rest of the 43S PIC components, including the 40S ribosomal subunit rRNA and proteins, are shown as semi-transparent ribbon. The possible contact surfaces for eIF5-CTD at the eIF1A-N-terminus (this work) and on the eIF1 surface (Luna et al., 2012) are circled and marked with dashed lines. (For interpretation of the references to color in this figure legend, the reader is referred to the Web version of this article.)

intriguing mechanistic questions about the effects it would have in the PIC. The much greater stimulation of eIF2β binding in the absence of the DWEAR motif, ~20-fold vs. 3-fold (Paul et al., 2022) indicates that CK2 phosphorylation could shift the equilibrium in favor of eIF2β binding when the DWEAR motif does not contact eIF5-CTD, while having little effect on the relative affinities of eIF2β and eIF1A in the presence of the DWEAR motif. The absence of the DWEAR motif would also expose the eIF1A-OB domain contact surface on eIF5-CTD, allowing eIF1A-OB binding. In contrast, eIF1A-NTT binding is not affected by the DWEAR motif position, but is instead mutually exclusive with eIF2β-NTT binding to eIF5-CTD.

The OB domain of eIF1A was recently found to interact with the eIF5B-CTD in 48S translation initiation complexes, mostly via loop 23, strand β3, and helix α3 (Brown et al., 2022; Lapointe et al., 2022). These surfaces do not overlap with the eIF1A – eIF5-CTD contact interfaces reported here. Intriguingly, eIF1A-OB contact surface on eIF5B-CTD partially overlaps with the previously reported contact surface for eIF1A-CTT (Marintchev et al., 2003; Zheng et al., 2014). Electron density

attributed to eIF1A-CTT binding to eIF5B-CTD was only observed in one of the 48S complex structures (Lapointe et al., 2022), but not the other (Brown et al., 2022), raising the question whether the two interactions occur at the same stages of translation initiation. However, mutational and kinetic experiments in *S. cerevisiae* have shown that the interaction mediated by eIF1A-CTT contributes to both ribosomal subunit joining and the coordinated release of eIF1A and eIF5B from the 80S ribosomal complex (Acker et al., 2006, 2009; Fringer et al., 2007).

In summary, our data shows that eIF5-CTD contacts eIF1A-OB at a surface that also binds to the 40S ribosomal subunit, and that the eIF5 DWEAR motif and eIF1A-CTT interfere with this interaction. eIF1A-NTT contacts eIF5-CTT, including the disordered C-terminal portion of AA-box 2, where the CK2 phosphorylation sites lie. Finally, CK2 phosphorylation of AA-box 2 stimulates binding to eIF1A. More work needs to be done to understand the role CK2 phosphorylation might have on the interactions of eIF5 with eIF1 and/or eIF3c, and on the overall architecture and stability of the MFC and the PIC.

## 4. Materials and methods

### 4.1. Protein expression and purification

All proteins used (Fig. 1) were human and expressed in *E. coli*. Expression and purification of recombinant $His_6$-tagged human eIF1A (Nag et al., 2016) and eIF5-CTD (Paul et al., 2022) constructs were as described previously. Briefly, eIF5-CTD constructs were expressed overnight at 20 °C, and purified in 300 mM KCl, and all eIF1A constructs were expressed for 3 h at 37 °C, and purified in 1 M KCl, except for the eIF1A OB domain, which was expressed at 20 °C for 3 h $^{15}N$ and $^{2}H$ labeling was achieved by growing bacteria in minimal medium supplemented with [$^{15}N$] $NH_4Cl$ and $^{2}H_2O$, respectively. Proteins were exchanged into buffer containing 10 mM Na Phosphate (pH 7.0), 150 mM KCl, 1 mM EDTA, 0.02% $NaN_3$, 1 mM DTT, and 0.1 mM AEBSF.

### 4.2. Nuclear magnetic resonance (NMR)

NMR experiments were performed in buffer containing 10 mM Na phosphate, pH 7.0, 150 mM KCl, 1 mM EDTA, 0.02% $NaN_3$, 1 mM DTT and 0.1 mM AEBSF, with 5% $^{2}H_2O$. NMR data were collected on a 500 MHz Bruker spectrometer (Boston University School of Medicine) equipped with a cryoprobe. NMR resonance assignments for eIF5-CTD, eIF1A, and their fragments were available (Battiste et al., 2000; Lin et al., 2018; Luna et al., 2012; Nag et al., 2016).

### 4.3. NMR chemical shift perturbation (CSP) assay

$^{15}N$ Transverse relaxation optimized spectroscopy heteronuclear single-quantum coherence (TROSY-HSQC) experiments with $^{15}N/^{2}H$-labeled proteins were used for the NMR chemical shift perturbation (CSP) assay. Chemical shift changes were calculated according to the formula $\delta = ((\delta_H)^2 + (\delta_N/5)^2)^{1/2}$ and affected residues were mapped on the surface of the protein. For statistical analysis, average chemical shift changes and standard deviations were calculated in Excel.

### 4.4. $K_D$ determination

To determine the affinity of the interactions, a $^{15}N/^{2}H$-labeled protein sample was titrated with increasing concentrations of an unlabeled binding partner, until saturation or until the solubility limit was reached. Chemical shift changes were plotted as a function of % maximum chemical shift. SigmaPlot was used to fit the data and calculate $K_D$s of binding, using a custom function taking into account that the concentration of the labeled protein is comparable to the $K_D$ and cannot be ignored: $f = \delta_{max}*((P + x + K_D - ((-P - x - K_D)^2 - 4*P*x)^{1/2})/(2*P))$, where $\delta_{max}$ is the maximum chemical shift change at saturation; P is the concentration of the labeled protein; and x is the concentration of the unlabeled binding partner. In eIF1A and eIF1A-NTT, fitting was done using the chemical shifts of a single NTT peak (G5). In eIF1A-ΔC, fitting was done using an average of the chemical shifts of several OB domain peaks; standard deviations are shown for those data points. To calculate averages from multiple peaks, the magnitude of the CSP at the highest concentration data point was used to normalize the lower concentration points because the magnitudes of the CSPs were, of course different for each individual peak. The magnitude of the CSP effects observed in eIF1A-ΔC with eIF5-CTD, particularly the phosphomimetic mutant, were much larger than those observed using full-length eIF1A, indicating that titrations using full-length eIF1A, including those reported previously (Paul et al., 2022), did not reach 50% binding, which is necessary to obtain a reliable fit, making the resulting fits unstable and sensitive to, e.g., self-association of the ligand at high concentrations. Therefore, to obtain reliable $K_D$s for the weaker interactions, we instead used the % binding obtained from the stronger interactions.

## CRediT authorship contribution statement

**Nathan Gamble:** Investigation, Formal analysis, Visualization, Writing – original draft, Writing – review & editing. **Eleanor Elise Paul:** Investigation, Formal analysis. **Bibin Anand:** Investigation, Formal analysis. **Assen Marintchev:** Conceptualization, Funding acquisition, Supervision, Methodology, Investigation, Formal analysis, Visualization, Writing – original draft, Writing – review & editing.

## Declaration of competing interest

The authors declare that they have no known competing financial interests or personal relationships that could have appeared to influence the work reported in this paper.

## Acknowledgments

This work was supported by the National Institute of Health [GM134113 to A.M.].

## Appendix A. Supplementary data

Supplementary data to this article can be found online at https://doi.org/10.1016/j.crstbi.2022.09.003.

## References

Acker, M.G., Shin, B.S., Dever, T.E., Lorsch, J.R., 2006. Interaction between eukaryotic initiation factors 1A and 5B is required for efficient ribosomal subunit joining. J. Biol. Chem. 281, 8469–8475.

Acker, M.G., Shin, B.S., Nanda, J.S., Saini, A.K., Dever, T.E., Lorsch, J.R., 2009. Kinetic analysis of late steps of eukaryotic translation initiation. J. Mol. Biol. 385, 491–506.

Asano, K., Clayton, J., Shalev, A., Hinnebusch, A.G., 2000. A multifactor complex of eukaryotic initiation factors, eIF1, eIF2, eIF3, eIF5, and initiator tRNA(Met) is an important translation initiation intermediate in vivo. Gene. Dev. 14, 2534–2546.

Asano, K., Krishnamoorthy, T., Phan, L., Pavitt, G.D., Hinnebusch, A.G., 1999. Conserved bipartite motifs in yeast eIF5 and eIF2Bepsilon, GTPase-activating and GDP-GTP exchange factors in translation initiation, mediate binding to their common substrate eIF2. EMBO J. 18, 1673–1688.

Aylett, C.H., Boehringer, D., Erzberger, J.P., Schaefer, T., Ban, N., 2015. Structure of a yeast 40S-eIF1-eIF1A-eIF3-eIF3j initiation complex. Nat. Struct. Mol. Biol. 22, 269–271.

Battiste, J.L., Pestova, T.V., Hellen, C.U., Wagner, G., 2000. The eIF1A solution structure reveals a large RNA-binding surface important for scanning function. Mol. Cell 5, 109–119.

Bieniossek, C., Schutz, P., Bumann, M., Limacher, A., Uson, I., Baumann, U., 2006. The crystal structure of the carboxy-terminal domain of human translation initiation factor eIF5. J. Mol. Biol. 360, 457–465.

Brown, Z.P., Abaeva, I.S., De, S., Hellen, C.U.T., Pestova, T.V., Frank, J., 2022. Molecular architecture of 40S translation initiation complexes on the hepatitis C virus IRES. EMBO J. 41, e110581.

Erzberger, J.P., Stengel, F., Pellarin, R., Zhang, S., Schaefer, T., Aylett, C.H.S., Cimermancic, P., Boehringer, D., Sali, A., Aebersold, R., Ban, N., 2014. Molecular architecture of the 40SeIF1eIF3 translation initiation complex. Cell 158, 1123–1135.

Fekete, C.A., Applefield, D.J., Blakely, S.A., Shirokikh, N., Pestova, T., Lorsch, J.R., Hinnebusch, A.G., 2005. The eIF1A C-terminal domain promotes initiation complex assembly, scanning and AUG selection in vivo. EMBO J. 24, 3588–3601.

Fringer, J.M., Acker, M.G., Fekete, C.A., Lorsch, J.R., Dever, T.E., 2007. Coupled release of eukaryotic translation initiation factors 5B and 1A from 80S ribosomes following subunit joining. Mol. Cell Biol. 27, 2384–2397.

Hashem, Y., des Georges, A., Dhote, V., Langlois, R., Liao, H.Y., Grassucci, R.A., Hellen, C.U., Pestova, T.V., Frank, J., 2013. Structure of the mammalian ribosomal 43S preinitiation complex bound to the scanning factor DHX29. Cell 153, 1108–1119.

Hinnebusch, A.G., 2014. The scanning mechanism of eukaryotic translation initiation. Annu. Rev. Biochem. 83, 779–812.

Homma, M.K., Wada, I., Suzuki, T., Yamaki, J., Krebs, E.G., Homma, Y., 2005. CK2 phosphorylation of eukaryotic translation initiation factor 5 potentiates cell cycle progression. Proc. Natl. Acad. Sci. U. S. A. 102, 15688–15693.

Hussain, T., Llacer, J.L., Fernandez, I.S., Munoz, A., Martin-Marcos, P., Savva, C.G., Lorsch, J.R., Hinnebusch, A.G., Ramakrishnan, V., 2014. Structural changes enable start codon recognition by the eukaryotic translation initiation complex. Cell 159, 597–607.

Jackson, R.J., Hellen, C.U., Pestova, T.V., 2010. The mechanism of eukaryotic translation initiation and principles of its regulation. Nat. Rev. Mol. Cell Biol. 11, 113–127.

Kratzat, H., Mackens-Kiani, T., Ameismeier, M., Potocnjak, M., Cheng, J., Dacheux, E., Namane, A., Berninghausen, O., Herzog, F., Fromont-Racine, M., Becker, T., Beckmann, R., 2021. A structural inventory of native ribosomal ABCE1-43S pre-initiation complexes. EMBO J. 40, e105179.

Lapointe, C.P., Grosely, R., Sokabe, M., Alvarado, C., Wang, J., Montabana, E., Villa, N., Shin, B.S., Dever, T.E., Fraser, C.S., Fernandez, I.S., Puglisi, J.D., 2022. eIF5B and eIF1A reorient initiator tRNA to allow ribosomal subunit joining. Nature 607, 185–190.

Lin, K.Y., Nag, N., Pestova, T.V., Marintchev, A., 2018. Human eIF5 and eIF1A Compete for Binding to eIF5B. Biochemistry 57, 5910–5920.

Llacer, J.L., Hussain, T., Dong, J., Villamayor, L., Gordiyenko, Y., Hinnebusch, A.G., 2021. Large-scale movement of eIF3 domains during translation initiation modulate start codon selection. Nucleic Acids Res. 49, 11491–11511.

Llacer, J.L., Hussain, T., Marler, L., Aitken, C.E., Thakur, A., Lorsch, J.R., Hinnebusch, A.G., Ramakrishnan, V., 2015. Conformational differences between open and closed states of the eukaryotic translation initiation complex. Mol. Cell 59, 399–412.

Llacer, J.L., Hussain, T., Saini, A.K., Nanda, J.S., Kaur, S., Gordiyenko, Y., Kumar, R., Hinnebusch, A.G., Lorsch, J.R., Ramakrishnan, V., 2018. Translational initiation factor eIF5 replaces eIF1 on the 40S ribosomal subunit to promote start-codon recognition. Elife 7.

Lomakin, I.B., Steitz, T.A., 2013. The initiation of mammalian protein synthesis and mRNA scanning mechanism. Nature 500, 307–311.

Luna, R.E., Arthanari, H., Hiraishi, H., Akabayov, B., Tang, L., Cox, C., Markus, M.A., Luna, L.E., Ikeda, Y., Watanabe, R., Bedoya, E., Yu, C., Alikhan, S., Wagner, G., Asano, K., 2013. The interaction between eukaryotic initiation factor 1A and eIF5 retains eIF1 within scanning preinitiation complexes. Biochemistry 52, 9510–9518.

Luna, R.E., Arthanari, H., Hiraishi, H., Nanda, J., Martin-Marcos, P., Markus, M.A., Akabayov, B., Milbradt, A.G., Luna, L.E., Seo, H.C., Hyberts, S.G., Fahmy, A., Reibarkh, M., Miles, D., Hagner, P.R., O'Day, E.M., Yi, T., Marintchev, A., Hinnebusch, A.G., Lorsch, J.R., et al., 2012. The C-terminal domain of eukaryotic initiation factor 5 promotes start codon recognition by its dynamic interplay with eIF1 and eIF2beta. Cell Rep. 1, 689–702.

Marintchev, A., Frueh, D., Wagner, G., 2007. NMR methods for studying protein-protein interactions involved in translation initiation. Methods Enzymol. 430, 283–331.

Marintchev, A., Kolupaeva, V.G., Pestova, T.V., Wagner, G., 2003. Mapping the binding interface between human eukaryotic initiation factors 1A and 5B: a new interaction between old partners. Proc. Natl. Acad. Sci. U. S. A. 100, 1535–1540.

Marintchev, A., Wagner, G., 2004. Translation initiation: structures, mechanisms and evolution. Q. Rev. Biophys. 37, 197–284.

Nag, N., Lin, K.Y., Edmonds, K.A., Yu, J., Nadkarni, D., Marintcheva, B., Marintchev, A., 2016. eIF1A/eIF5B interaction network and its functions in translation initiation complex assembly and remodeling. Nucleic Acids Res. 44, 7441–7456.

Obayashi, E., Luna, R.E., Nagata, T., Martin-Marcos, P., Hiraishi, H., Singh, C.R., Erzberger, J.P., Zhang, F., Arthanari, H., Morris, J., Pellarin, R., Moore, C., Harmon, I., Papadopoulos, E., Yoshida, H., Nasr, M.L., Unzai, S., Thompson, B., Aube, E., Hustak, S., et al., 2017. Molecular landscape of the ribosome pre-initiation complex during mRNA scanning: structural role for eIF3c and its control by eIF5. Cell Rep. 18, 2651–2663.

Olsen, D.S., Savner, E.M., Mathew, A., Zhang, F., Krishnamoorthy, T., Phan, L., Hinnebusch, A.G., 2003. Domains of eIF1A that mediate binding to eIF2, eIF3 and eIF5B and promote ternary complex recruitment in vivo. EMBO J. 22, 193–204.

Paul, E.E., Lin, K.Y., Gamble, N., Tsai, A.W., Swan, S.H.K., Yang, Y., Doran, M., Marintchev, A., 2022. Dynamic interaction network involving the conserved intrinsically disordered regions in human eIF5. Biophys. Chem. 281, 106740.

Saini, A.K., Nanda, J.S., Lorsch, J.R., Hinnebusch, A.G., 2010. Regulatory elements in eIF1A control the fidelity of start codon selection by modulating tRNA(i)(Met) binding to the ribosome. Gene. Dev. 24, 97–110.

Simonetti, A., Guca, E., Bochler, A., Kuhn, L., Hashem, Y., 2020. Structural insights into the mammalian late-stage initiation complexes. Cell Rep. 31, 107497.

Sokabe, M., Fraser, C.S., Hershey, J.W., 2012. The human translation initiation multi-factor complex promotes methionyl-tRNAi binding to the 40S ribosomal subunit. Nucleic Acids Res. 40, 905–913.

Sonenberg, N., Hinnebusch, A.G., 2009. Regulation of translation initiation in eukaryotes: mechanisms and biological targets. Cell 136, 731–745.

Weisser, M., Ban, N., 2019. Extensions, extra factors, and extreme complexity: ribosomal structures provide insights into eukaryotic translation. Cold Spring Harbor Perspect. Biol. 11.

Weisser, M., Voigts-Hoffmann, F., Rabl, J., Leibundgut, M., Ban, N., 2013. The crystal structure of the eukaryotic 40S ribosomal subunit in complex with eIF1 and eIF1A. Nat. Struct. Mol. Biol. 20, 1015–1017.

Yamamoto, Y., Singh, C.R., Marintchev, A., Hall, N.S., Hannig, E.M., Wagner, G., Asano, K., 2005. The eukaryotic initiation factor (eIF) 5 HEAT domain mediates multifactor assembly and scanning with distinct interfaces to eIF1, eIF2, eIF3, and eIF4G. Proc. Natl. Acad. Sci. U. S. A. 102, 16164–16169.

Yi, S.H., Petrychenko, V., Schliep, J.E., Goyal, A., Linden, A., Chari, A., Urlaub, H., Stark, H., Rodnina, M.V., Adio, S., Fischer, N., 2022. Conformational rearrangements upon start codon recognition in human 48S translation initiation complex. Nucleic Acids Res. 50, 5282–5298.

Yu, Y., Marintchev, A., Kolupaeva, V.G., Unbehaun, A., Veryasova, T., Lai, S.C., Hong, P., Wagner, G., Hellen, C.U., Pestova, T.V., 2009. Position of eukaryotic translation initiation factor eIF1A on the 40S ribosomal subunit mapped by directed hydroxyl radical probing. Nucleic Acids Res. 37, 5167–5182.

Zheng, A., Yu, J., Yamamoto, R., Ose, T., Tanaka, I., Yao, M., 2014. X-ray structures of eIF5B and the eIF5B-eIF1A complex: the conformational flexibility of eIF5B is restricted on the ribosome by interaction with eIF1A. Acta. Crystallogr. D Biol. Crystallogr. 70, 3090–3098.